International Journal of Engineering Trends and Technology
ISSN: 2231-5381/ https://doi.org/10.14445/22315381/IJETT-V74I5P103

Volume 74 Issue 5, 35-51, May 2026

Original Article

Visual Interpretability in Glaucoma Detection Using Grad-CAM-Driven Transfer Learning

Z Abdul Basith[1], M Sulthan Ibrahim[2]

[1]*Department of Computer Applications, Madurai Kamaraj University (MKU), Madurai, India.*
[2]*Department of Computer Science, Government Arts and Science College, Affiliated to Madurai Kamaraj University, India.*

[1]*Corresponding Author : abdbasith93@gmail.com*

Received:17 November 2025 Revised: 03 March 2026 Accepted: 11 March 2026 Published: 30 May 2026

Abstract - *Glaucoma is a progressive eye disease characterized by damage to the optic nerve. Early detection and management are crucial to preserving vision, making the prediction of glaucoma risk. To improve accurate prediction, a Gradient-weighted Class Activation Mapped Deep Transfer Learning (GWCAMDTL) model is developed with higher accuracy of glaucoma prediction and lesser time. Retinal fundus images are collected from a dataset in image acquisition. Deep transfer learning involves adapting a pre-trained deep learning model for performing glaucoma prediction. Initially, layers in the pre-trained model are usually frozen to preserve the learned features from the infected regions. Transferring information from previously learned results by the pre-trained mode to new tasks has the potential to significantly improve feature learning efficiency by the congruence correlation coefficient. Gradient-weighted Class Activation Mapping generates visual explanations for predictions made by the model. Fine-tuning layers is a crucial part of transfer learning. During fine-tuning for glaucoma prediction, the model weights of certain layers are updated to better fit specific characteristics of the new glaucoma dataset, leading to a reduction in both training and validation error. This approach improves the accuracy of glaucoma prediction by applying the strengths of the pre-trained model and adapting it to the clinical features of retinal fundus images. Experiments are conducted using various evaluation metrics. Results of GWCAMDTL achieve higher accuracy by 96%, precision by 0.95, sensitivity by 0.96, F1 score by 0.95, and specificity by 0.93 with reduced time by 27% as well as error by 0.042 than existing methods.*

Keywords - *Glaucoma Disease Prediction, Deep Transfer Learning, Multilayer Perceptron Classifier, Congruence Correlation Coefficient, Gradient-Weighted Class Activation Mapping.*

1. Introduction

Glaucoma is the second leading cause of blindness worldwide, and it poses a significant public health challenge. The Glaucoma Domain Adaptation model (GDA) was developed [1] for glaucoma diagnosis. However, GDA did not utilize a more robust deep learning model for training with a larger dataset. A hybrid glaucoma detection framework was developed [2] to perform predictions. However, it consumes more time. An automated glaucoma detection method was developed in [3] using an ensemble of random forest classifiers. The Glaucoma Diagnosis Network was developed in [4] for optic disk localization. A new multi-task deep learning approach was developed [5] for accurate glaucoma diagnosis. CNN was developed [6] for glaucoma detection. A deep CNN model was developed [7] for visualizing features related to glaucoma diagnosis. Two networks, named the Segmentation Network and the Segmentation Residual Network, were developed [8]. A new feature, an excitation-based dense segmentation network model, was developed [9]. An automated classification algorithm was developed [10] using fundus photographs. An intelligent computer-aided system was developed [11] using DNN. The DL technique was developed [12]. Hybrid techniques were developed [13] for classifying eye diseases. An Artificial Intelligence (AI) and Deep Learning Model (DL) was developed in [14] for glaucoma management. A novel computational model was designed [15] to achieve high accuracy. However, it was unable to identify the severity of the glaucoma condition.

1.1. Research Gap

Glaucoma is a chronic neurological illness in the retina that causes vision loss. By using retinal fundus images, the glaucoma disease recognition is carried out. A fundus image is an image of the eye confined by a specific fundus camera, which contains a mixture of structural and textural features. There are many methods that have been designed for Glaucoma disease detection. Early detection is vital in glaucoma disease. Early detection greatly reduces the risk of further vision loss. Several methods were designed for glaucoma detection. Due to the time-consuming, inaccurate, and manual nature of traditional methods, automation in glaucoma detection is vital. To address the issue, the

GWCAMDTL method was introduced. Contrary to conventional methods,

1.2. Novelty and Contributions

- To enhance glaucoma disease prediction accuracy, the GWCAMDTL method was developed.
- To minimize disease prediction time, a novel transfer learning model performs preprocessing, segmentation, and feature extraction. Camargo's Indexive Total Variation Regularization method is used to enhance image quality. Following this, the Wald Statistics Diagonal Connectivity Test is employed for segmenting the Region of Interest (ROI), after which clinical features are extracted.
- To enhance accuracy and minimize error, the Congruence Coefficient is used to measure the similarity and analyze feature vectors for predicting the level of glaucoma disease.
- To produce multiple classification outcomes, the softmax activation function is applied to the resulting coefficient values.
- Fine-tuning process of deep transfer learning model reduces error rate and improves accuracy.
- Experimental assessment is conducted to evaluate the performance of the GWCAMDTL method using various metrics and comparing it to other deep learning methods.

1.3. Organization of Paper

The paper is organized as follows: Section 2 reviews related work. Section 3 describes the GWCAMDTL method. Section 4 outlines the experimental setup. Section 5 presents a comparative analysis. Section 6 provides a conclusion.

2. Related works

Attention mechanisms were designed in [16] to learn features for eye disease detection, significantly enhancing performance. However, these mechanisms did not improve classification performance by effectively utilizing fundus structures. A glaucoma forecasting transformer model was developed [17] to predict glaucoma. However, the model was trained using a dataset with a limited number of glaucoma cases. The Multi-Scale Transfer Learning framework (MTRA-CNN) was developed [18] for graded diagnosis. However, the framework faced challenges in reducing complexity and improving performance across multi-stage transfer learning processes. A multi-stage ensemble-based system was designed in [19] for diagnosing glaucomatous. However, it did not utilize multimodal data for validation for more reliable predictions. A robust and accurate automated system was developed [20] using DL. However, the model did not perform fine-tuning of the deep learning algorithms to improve its performance further. A new IoT and DL enabled diabetic retinopathy diagnosis model was developed [21]. This model utilizes IoT devices to achieve minimal computation time for diagnosing diabetic retinopathy. High-Resolution Network (HRNet) was developed [22] to enhance quality. However, it did not significantly improve the system's generalization and robustness. A random forest classifier model was developed [23] to classify retinal fundus images. However, the model was unable to apply different combinations of filters with a reduced feature set.

Table 1. Comparison of existing methods

Reference. No	Method	Objectives	Metris	Demerits
[1]	GDA	To obtain a glaucoma diagnosis and glaucoma forecasting	Higher accuracy	GDA did not utilize robust DL
[2]	Hybrid glaucoma detection framework	To perform predictions	Enhance patient outcomes	It consumes more time
[6]	CNN	To find glaucoma	Lesser time	Failed to handle larger fundus images
[12]	Deep learning technique	To segment and classify fundus images	Higher precision	It did not extend its experiments
[18]	MTRA-CNN	To achieve an effective graded diagnosis	Increase accuracy	It failed to reduce complexity
[25]	Automatic method	To detect early-stage glaucoma	Higher accuracy	It failed to diagnose early-stage glaucoma
[28]	U-Net CNN	To determine glaucoma	Lesser time	It failed to develop intelligent, fully automated applications
[29]	Activation function	To diagnose glaucoma	Reduce error	The complexity of the model was not reduced
[30]	Multiple image processing and DL methods	To determine glaucoma	Higher accuracy	It failed to handle a large dataset
[32]	Ensemble learning with three DL models	To predict glaucoma	Lesser time	Segmentation was not performed

The DL framework was developed [24] by a generative algorithm. An automatic method was developed in [25] for early-stage glaucoma. A novel multimodal neural network was developed [26] for classifying glaucoma with minimal loss. An explainable AI model [27] and U-Net CNN architecture were designed in [28] for detecting glaucoma. A deep CNN was developed [7] through feature visualization.

However, the prediction accuracy was not improved. An efficient activation function for CNN models was developed [29]. However, the complexity of the model was not reduced. Multiple image processing and DL methods were designed [30] for glaucoma detection and enhancing accuracy. However, it failed to handle a large dataset. CNN-Based Ensemble DL for Glaucoma Detection and Staging Using Retinal Fundus Images, named E-GlauNet, was developed [31] in less time.

However, the time was higher. Ensemble learning with three deep learning models was introduced in [32] to detect glaucoma in less time. However, segmentation was not performed to enhance accuracy. Table 1 describes a comparison of existing methods. Compared to existing methods, the proposed GWCAMDTL offers a balanced trade-off between accuracy, precision, sensitivity, and time. A transfer learning model constructs a pre-trained classifier using training images. A Multilayer Perceptron (MLP) classifier is utilized as the pre-trained model, which includes various layers. Image preprocessing is performed to enhance image quality by removing noise. Clinical features are extracted from the ROI. The congruence correlation coefficient is used to analyze the extracted features. Softmax activation function is applied to the resulting coefficient values to produce multiple classification outcomes. Finally, fine-tuning of the newly added layers is performed with minimum error. Accurate disease prediction results obtained with minimal time and error have higher accuracy.

3. Proposal methodology

The purpose of the GWCAMDTL model is to enhance the early detection of glaucoma by analyzing various types of features and identifying potential symptoms before they become severe.

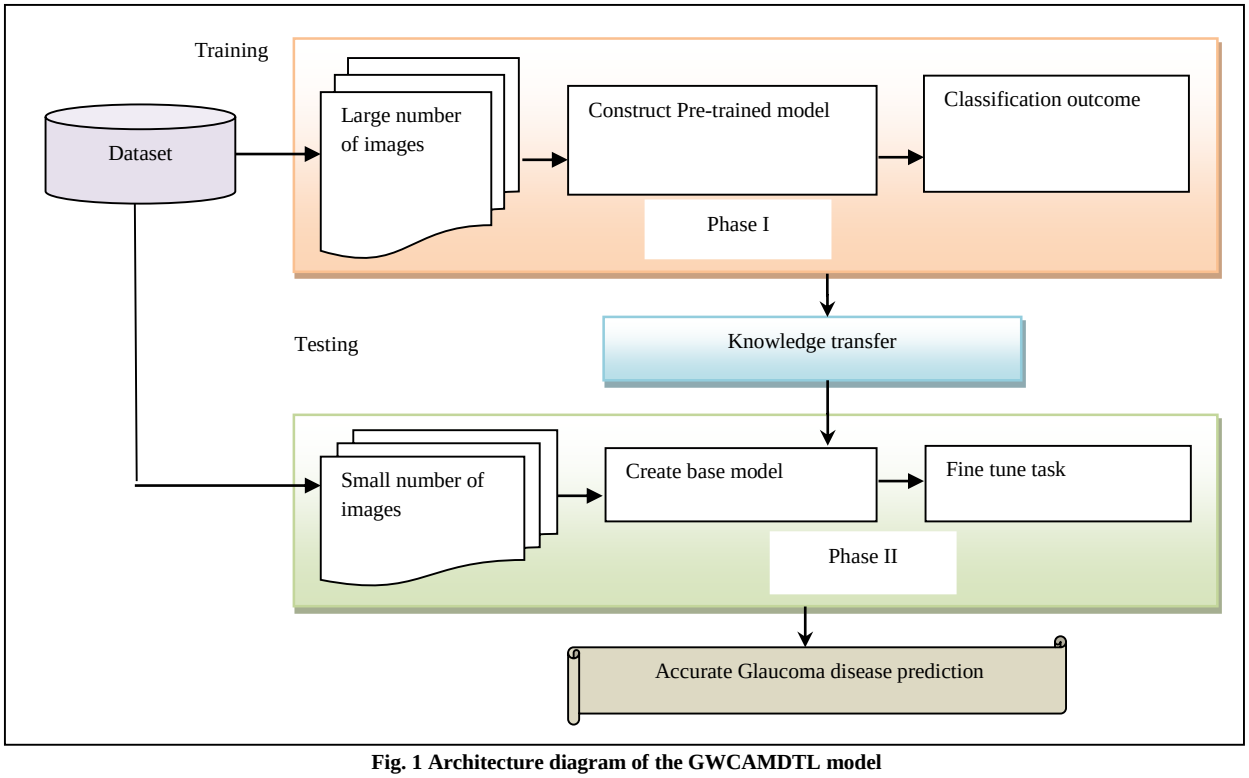

Fig. 1 Architecture diagram of the GWCAMDTL model

Figure 1 shows the architecture diagram of the proposed GWCAMDTL model using two phases. In the initial phase, the pre-trained model is constructed with a large number of training sample images. The base model is created with the knowledge of the pre-trained model in phase 2. The phases include the different fundamental processes, namely data acquisition, preprocessing, feature extraction, and classification.

3.1. Image Acquisition

In the GWCAMDTL model, image acquisition refers to the process of capturing and collecting medical fundus images to assist in the early detection and diagnosis of glaucoma. The

Glaucoma Fundus Imaging Dataset is used for collecting the numerous fundus images taken from https://www.kaggle.com/datasets/arnavjain1/glaucoma-datasets. This dataset comprises a collection of fundus images and corresponding optic disc/cup segmentations and Glaucoma diagnosis information.

3.2. Transfer Learning Model

After data acquisition, Transfer Learning (TL) is a machine learning technique in which knowledge learned from a pre-trained model is reused in order to boost the performance of prediction. For image classification, Transfer learning provides significant advantages, including reduced training time, improved performance, and enhanced model capabilities.

3.2.1. Construct a Pre-Trained Model

In a transfer learning model, the first process is to construct a pre-trained model that significantly enhances the efficiency and accuracy of diagnosing the condition by utilizing the deep learning models trained on large datasets.

A Multilayer Perceptron (MLP) is used as a pre-trained model for glaucoma detection. An MLP is a type of deep learning technique consisting of multiple layers of neurons, including an input layer, one or more hidden layers, and an output layer. Each neuron in one layer is connected to every neuron in the next layer, making it a fully connected network.

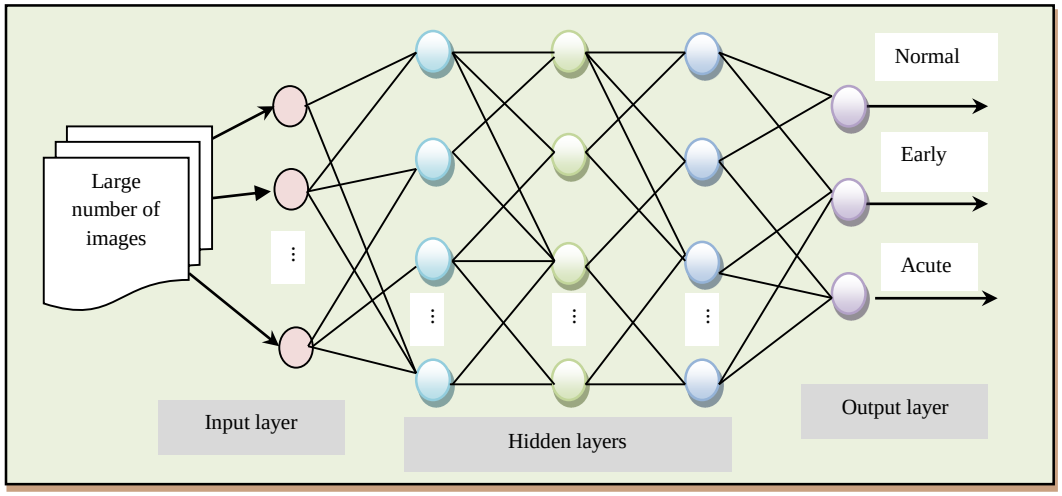

Fig. 2 Schematic structure of Multilayer Perceptron classifier

Figure 2 depicts the schematic structure of the Multilayer Perceptron classifier, which consists of three layers. The input and output layers are always single layers, while hidden layers include numerous sublayers. Each layer of a neural network is composed of small units known as artificial neurons, perceptrons, or nodes. Each artificial neuron processes weighted inputs, applies an activation function, and forwards the output to other neurons in the network. Connections between these neurons, known as synapses, have associated weights that influence the strength of data passed between neurons. The Multilayer Perceptron classifier considers the training set. $\{X_i, Y_j\}$where X_i denotes training sample fundus images'$SI=\{SI_1, SI_2, ...,SI_n\}$' and Y_j indicates a classification outcome. The number of sample fundus images is provided as input to the input layer of the Multilayer Perceptron (MLP) classifier. Each neuron in the input layer receives these sample fundus images and forwards them to the hidden layer, applying corresponding weights and biases. Each neuron in the hidden layer computes a weighted sum of inputs it receives from the input layer. If *SI* represents the input from a neuron of the input layer, the weighted sum for the neuron is computed,

$$Q = \sum_{i=1}^{n} (SI_i * \beta_{ij}) + b_j \quad (1)$$

Where Q is a weighted sum function, SI_i denotes a sample fundus image, β_{ij} is the weight associated with the connection between neuron iin input layer and neuron j in the hidden layer, and b_j is the bias for neuron j. Apply an activation function before passing the results to the hidden layer. Weighted sum Q is then passed through an activation function F to determine the neuron's final output.

$$W = F(Q) = \begin{cases} 0, & \&Q<0 \\ 1, & Q\geq 0 \end{cases} \quad (2)$$

Where *F* is a binary activation function applied to the weighted sum *Q*. If a neuron in a neural network is considered active and produces an output of 1, this typically means the neuron's activation function has produced a high value. Input is transferred into the first hidden layer through active neurons. In that layer, image preprocessing is performed for enhancing image quality by removing noisy pixels. Camargo's indexive total variation regularization method is employed for image denoising. Total Variation (TV)

regularization is a method used in image processing tasks to remove noise while preserving important features such as edges. The method is based on the concept of minimizing the total variation of an image, which helps smooth out noise while maintaining sharp edges. Consider the input image. SI_1, SI_2, ...,SI_n. The number of pixels in each image is represented as P_1,P_2,P_3...P_m. Proposed technique window with size of $k*k$. Pixels are arranged into a filtering window,

P_1	P_2	P_3
P_4	P_5	P_6
P_7	P_8	P_9

Fig. 3 *k*k*Filtering window

Figure 3 illustrates k*k filtering windows, where pixels P_1,P_2,P_3...P_m They are arranged in rows and columns. After, pixels are rearranged in increasing order. Absolute difference or total variation between pixels and neighboring pixels is determined using the following Camargo's index functions,

$$C=1-\frac{|P_j-P_n|}{m} \quad (3)$$

Where C is Camargo's index function's outcome, P_j is pixel in the increasing order, P_n denotes a neighboring pixel in the filtering window. Camargo's index test provides outcomes ranging from 0 to 1. When the value of Camargo's index function test is 1, the pixels are considered normal. Otherwise, pixels with more deviation are identified as noisy and are smoothed by the average value of other pixels,

$$P_N=\sum_{j=1}^{m}\frac{P_j}{m} \quad (4)$$

Where, P_N is a smoothed image of pixels, P_j represents pixels in the filtering window, m denotes the total number of pixels within the filtering window. Noisy pixels are removed and replaced with smoothed values based on an average value. Image preprocessing is performed to enhance fundus image quality. Then the preprocessed images are sent to the next hidden layer for segmenting the ROI from the input images. Segmentation in image processing, particularly in medical imaging, involves dividing an image into distinct regions that help identify Regions Of Interest (ROIs) such as specific tissues. This method segments an image by grouping neighboring pixels with similar intensity properties. The Wald statistics diagonal connectivity test is employed to group the pixels into regions based on their connectivity properties. This method is particularly useful for segmenting Regions Of Interest (ROIs) in an image where pixels are spatially relevant.

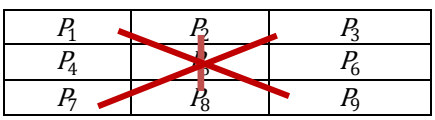

Fig. 4 Diagonal pixels connectivity

Figure 4 depicts diagonal pixel connectivity, which is represented by a red line. First, the starting point is marked with a central pixel located in two-dimensional space ($P_{x,y}$). Diagonal pixel connectivity is measured using the Wald statistical test between pixels.

$$WS=\frac{|P_{x,y}-P_D|}{\sigma} \quad (5)$$

WS is the Wald statistical test between pixels $P_{x,y}$ and P_D, σ is variation, $|P_{x,y}-P_D|$ is the distance between the centers $P_{x,y}$' and neighborhood pixels. ' P_D '. Pixels with minimal difference are selected as neighboring pixels.

$$S=\arg\min\{WS\} \quad (6)$$

From (11), 'S' denotes a connectivity between the pixel intensity, arg min denotes an argument of minimum function, it indicates a minimal distance between the two pixels, such as the center pixel's intensity '$P_{x,y}$'and other pixels' intensity. ' P_D '. The pixels around the center pixels' intensity are segmented to form the ROI region. After segmenting the ROI, the significant optic features, such as CDR, NRR, and BVR, and Retinal Nerve Fiber Layer (RNFL) Thickness, are extracted for accurate disease classification. The Optic Cup-To-Disc Ratio (CDR) is a crucial metric in the detection and management of glaucoma. Quantitatively assessing the CDR offers valuable insights for identifying individuals at risk of glaucoma and tracking the progression of the disease. The CDR is calculated as the ratio of the area of the Optic Cup (OC) to the area of the Optic Disc (OD),

$$CDR=2*\left[\frac{Area_{cup}[Res]}{Area_{disc}[Res]}\right] \quad (7)$$

Where CDR denotes a cup-to-disc ratio, $Area_{cup}[Res]$ denotes an area of cup and. '$Area_{disc}$' denotes an area of disc with resultant images obtained ' Res '. Neuroretinal Rim (NRR) is the area around Optic Nerve Head (ONH) where the axons of retinal cyst cells converge to form the optic nerve fiber layer. It represents the disc of tissue surrounding the optic cup within the optic disc.

$$Nrr=Nrr_{IQA}+\frac{Nrr_{SQA}}{Nrr_{NQA}}+Nrr_{TQA} \quad (8)$$

Where 'Nrr_{IQA}' indicates the Nrr in the Inferior quadrant area. 'Nrr_{SQA}' point out Nrr in the Superior Quadrant Area. 'Nrr_{NQA} ' represents Nrr in Nasal Quadrant Area,'Nrr_{TQA}' is Temporal Quadrant Area. The Blood Vessel Ratio 'BVR' offers a detailed evaluation of the distribution of blood vessels throughout the optic disc. This ratio is computed as the ratio of summing the BVR values from the Inferior and Superior Quadrant Areas and dividing it by the sum of the BVR values from the Nasal and Temporal Quadrant Areas.

$$Bvr=\left[\frac{BVR_{IQA}+BVR_{SQA}}{BVR_{NQA}+BVR_{TQA}}\right] \quad (9)$$

Where 'Bvr_{IQA}' designates the BVR in the Inferior Quadrant Area Bvr_{SQA}' indicates BVR in the Superior Quadrant Area. 'Bvr_{NQA}' signifies BVR in Nasal Quadrant Area and 'Bvr_{TQA}' represents BVR in Temporal Quadrant Area. Retinal Nerve Fiber Layer (RNFL) thickness is defined as the distance between the Inner Limiting Membrane (ILM) and the outer boundary of the innermost highly reflective layer.

$$RNFL=\left|y_{ILM}-y_{B\_RNFL}\right| \quad (10)$$

Where, y_{ILM} denotes a vertical position of the inner limiting membrane, y_{B_RNFL} indicates a vertical position of the outer boundary of the RNFL. Finally, these extracted features are analyzed with the testing feature value to obtain the final classification results. In the third hidden layer, the feature analysis is performed using the congruence coefficient. In multivariate statistics, the congruence coefficient is used to measure the similarity between factors derived from factor analysis. The congruence coefficient is used to measure the similarity of extracted factors across different samples. The similarity between the two feature vectors is estimated,

$$CC=\frac{\sum F_{EV}*F_{TV}}{\sqrt{\sum F_{EV}{}^2 \sum F_{TV}{}^2}} \quad (11)$$

Where CC designates the congruence correlation coefficient, F_{EV} denotes an extracted feature vector, F_{TV} indicates a prestored feature vector, $\sum F_{EV}*F_{TV}$ indicates a sum of the product of the paired scores of two features, $\sum F_{EV}{}^2$ symbolizes a squared score of F_{EV} and $\sum F_{TV}{}^2$ indicates a squared score of F_{TV}. The Congruence Coefficient (CC) yields values ranging from −1 to +1. A coefficient of '+1' is a perfect match between two features, meaning they are highly similar. The coefficient of '−1'is complete mismatch, indicating that the features are dissimilar. Based on the congruence coefficient output, the input fundus images are classified as either normal, early glaucoma, or acute glaucoma. These classified results are obtained at the output layer.

$$Y=F_{sof}\left(H_o\beta_{jk}\right) \quad (12)$$

$$F_{sof}=\frac{e^{CC_k}}{\sum_{k=1}^{c} e^{CC_k}} \quad (13)$$

Where Y is the output of the classifier, i.e., pre-trained model, F_{sof} is the softmax activation function, H_o is the output of hidden layers, β_{jk} is the weight associated with the connection between neuron jin hidden layer and neuron 'k' in the output layer. Softmax activation function, CC_k denotes a congruence coefficient for the k^{th} class, e denotes an exponential function applied to the k^{th} class, $\sum_{k=1}^{c} e^{CC_k}$ denotes a sum of the exponential functions applied to the k^{th} An efficient class. This result provides the final multi-classification results at the output layer.

3.2.2. Create the base Model

In a transfer learning model, a small number of testing images are taken as input to construct the new tasks by using the same base model, which is utilized in a pre-trained model (i.e., a deep multilayer perceptron deep learning model), and perform the new specific prediction tasks. In transfer learning, 'freeze layers' refer to layers in a pre-trained model that are not updated during the construction of the new model. Freezing layers is a technique used to retain the learned features of the pre-trained model while adapting the remaining layers to your specific task.

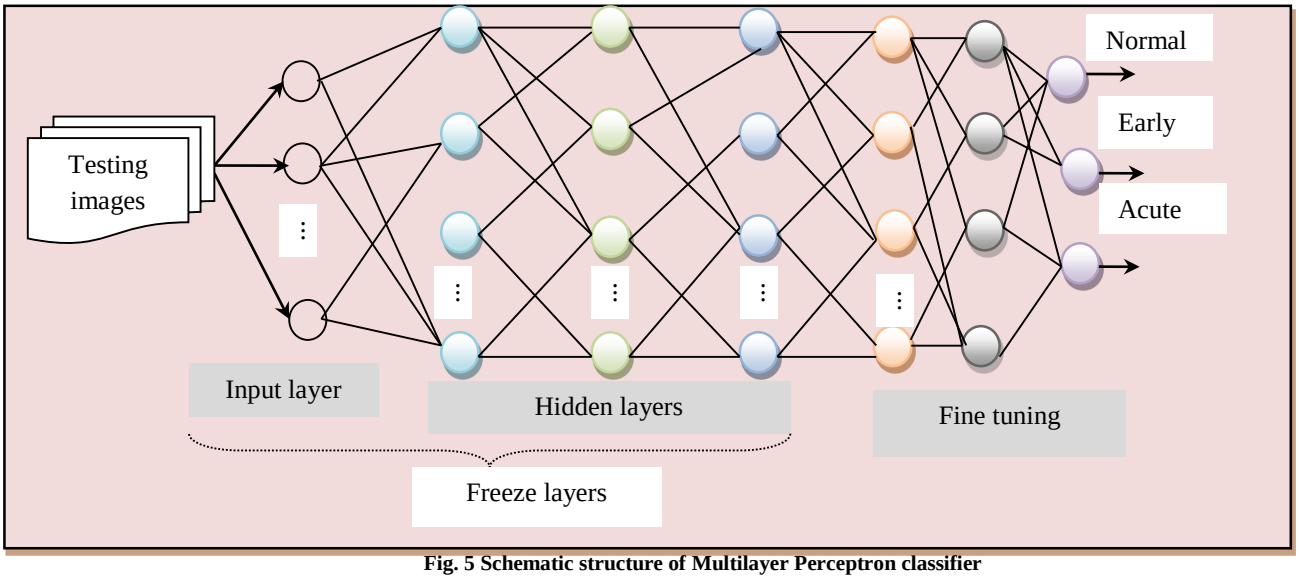

Fig. 5 Schematic structure of Multilayer Perceptron classifier

Figure 5 depicts the schematic structure of a Multilayer Perceptron classifier, which has frozen layers that selectively train certain layers of a neural network while keeping others unchanged. The main reason to freeze these layers is to control the knowledge and features learned from the pre-training model. The initial layers and three hidden layers of a pre-trained model are unchanged while processing the testing images. The main advantages of these freeze layers significantly enhance the speed of the training process and minimize the classification time. In phase 2, the network architecture consists of three types of layers: An Input Layer, One or More Hidden (Middle) Layers, and an Output Layer. The input and three hidden layers are a frozen layer, and adding two new layers for performing gradient mapping and a fine-tuning process to minimize the classification error.

The input small number of testing images is transferred into the hidden layers, where the image preprocessing steps are performed by utilizing the same model as Camargo's indexive total variation regularization method for enhancing the image quality by removing the noise artifacts. Followed by the multiple optic features such as CDR, NRR, and BVR, the Retinal Nerve Fiber Layer (RNFL) thickness is extracted from the preprocessed images. Then, the extracted features from the preprocessed test images and the information from the pre-trained model are analyzed by applying the congruence correlation coefficient. The similarity between the extracted features from the preprocessed test images and features learned from the pre-trained model is estimated as follows,

$$CC=\frac{\sum F_{EV(t)}*F_{EV}}{\sqrt{\sum F_{EV(t)}{}^2 \sum F_{EV}{}^2}} \tag{14}$$

Where CC designates the congruence correlation coefficient, $F_{EV(t)}$ denotes an extracted feature vector for the testing image, F_{EV} indicates an extracted feature vector from a pre-trained model, $\sum F_{EV(t)}*F_{EV}$ indicates a sum of the product of the paired scores of two features, $\sum F_{EV(t)}$ symbolizes a squared score of $F_{EV(t)}$ and $\sum F_{EV}{}^2$ indicates a squared score of F_{EV}. CC yields values ranging from −1 to +1. A coefficient of '+1' is a perfect match between the two features, meaning they are highly similar.

Conversely, a coefficient of '−1' signifies a indicating that the extracted features are dissimilar. Based on the feature matching, accurate classifications of normal, early glaucoma, and acute glaucoma are correctly detected. Based on the similarity measure, input fundus images are classified as either normal, early glaucoma, or acute glaucoma by the softmax activation function.

$$Y_n=F_{sof}\left(H_{o\,(n)}\beta_{jl(n)}\right) \tag{15}$$

$$F_{sof}=\frac{e^{CC_{b(n)}}}{\sum_{k=1}^{c} e^{CC_{k(n)}}} \tag{16}$$

Where, Y_n denotes an output of the classifier, i.e., a new model, F_{sof} indicates a softmax activation function, $H_{o\,(n)}$ denotes an output of hidden layers in the new model, $\beta_{jl(n)}$ denotes a weight associated with the connection between neuron jin in the hidden layer and neuron 'l in the output layer of the new model, $CC_{k(n)}$ denotes a congruence coefficient for the k^{th} class, e denotes an exponential function applied to the k^{th} class, $\sum_{k=1}^{c} e^{CC_{k(n)}}$ denotes a sum of the exponential functions applied to the k^{th} class. This result provides the final multi-classification results.

Based on the obtained information, the gradient-weighted class activation mapping function is employed for highlighting the infected regions that are important for the model's decision, providing interpretability to the predictions. It generates class activation maps without the need for additional backward passes through the network, making it computationally efficient. It utilizes the inherent spatial localization of the image pixels to highlight important infected regions in an image, enabling the network to focus on the relevant parts for each class prediction. Grad-CAM highlights the regions in the input image that are most relevant for predicting a specific class using the gradients of the output class score concerning the activations of neurons in the hidden layer. For a specific class k, the gradient of each class is measured as follows,

$$\nabla k=\frac{\partial Y_n{}^k}{\partial F_{sof}(j)} \tag{17}$$

Where ∇k denotes a gradient of each class ' k ', $Y_n{}^k$ denotes an output for class'k', $F_{sof}(j)$ indicates a softmax activation of neuron 'j' in the hidden layer of the feature map. The gradients are used to identify how important each neuron in the hidden layer is for the output class. To create a class activation map, weight the activations of neurons in the hidden layer by their corresponding gradients.

$$\beta^k(f)=\frac{1}{P_n}\sum\sum\frac{\partial Y_n{}^k}{\partial F_{sof}(j)} \tag{18}$$

Where, $\beta^k(F)$ denotes a weight for the feature map with respect to class 'k', P_n denotes a number of pixels in each feature map, $\frac{\partial Y_n{}^k}{\partial F_{sof}(j)}$ denotes a gradient of class 'k' with respect to the activation in the hidden layer '$F_{sof}(j)$' in the feature map. Finally, the class activation map is obtained as follows,

$$Z_k=RELU\left(\sum_k \beta^k(f)*F_{sof}(j)\right) \tag{19}$$

Where, Z_k denotes a class activation map, which provides a visual representation that indicates which parts of the input images are most infected in glaucoma disease for the prediction of class k. RELU denotes a Rectified Linear Unit (ReLU) activation function applied to ensure that only

positive contributions are considered in the class activation map. A negative value is typically not useful for visualization, $\beta^k(f)$ denotes an importance weight for the feature map with respect to class k, $F_{sof}(j)$ represents the activation map of the feature map, and represents the output of the neurons in j^{th} hidden layer after applying the activation function (such as ReLU).

3.2.3. Fine-tuning of the transfer learning

In transfer learning, fine-tuning is a process where a pre-trained model, which was trained on a large, general dataset, is adapted for a specific task by making adjustments to its hyperparameters. Fine-tuning helps the model utilize the knowledge gained from initial training to improve performance. The fine-tuning process is executed for updating weights between newly added layers to minimize error and enhance disease prediction accuracy. For each outcome, the error rate is computed based on the squared difference between the actual outcome and the prediction results.

$$\varepsilon=\left[Y_{Act}-Y_{pre}\right]^2 \quad (20)$$

Where, ERR is the actual classification results 'Y_{Act}', Y_{pre} is predicted classification outcomes. During fine-tuning, error back-propagation algorithms adjust hyperparameters (i.e., weights) optimally to increase accuracy.

$$\beta_{t+1}=\beta_t-\eta\left[\frac{\partial\varepsilon}{\partial w_t}\right] \quad (21)$$

Where, β_{t+1} indicates an updated weight, β_t indicates a current weight, η denotes a learning rate $(\eta<1)$, '$\frac{\partial\varepsilon}{\partial w_t}$' represents a partial derivative of the error 'ε' with respect to the current weight. 'β_t'. The above-mentioned updating process is repeated until a minimum error. Finally, accurate disease prediction results with the infected regions visualization are obtained at the output layer, which improves the disease prediction.

// Algorithm 1: Gradient-weighted Class Activation Mapped Deep Transfer Learning
Input: Dataset, fundus images $SI_1, SI_2, SI_3, \ldots SI_n$ Output: Increase the disease prediction accuracy
Begin 1. Construct the pre-trained model 2. Collect a number of training fundus images $SI_1, SI_2, SI_3, \ldots SI_n$ taken at the input layer 3. For each training image SI 4. Formulate the neuron activation probability using (2) 5. Preprocessing the input image using (3) (4) –[hidden layer 1] 6. Segment the ROI using (5) (6) 7. Extracts the clinical features using (7)(8)(9)(10) 8. End for extracted feature vector, F_{TV} indicates a prestored feature vector 9. For each feature vector 'FE' 10. For each pre-stored feature vector. 'F_{TV}' 11. Measure the congruence correlation coefficient using (11) 12. End for 13. End for 14. Apply the softmax activation function using (17) to obtain classification outcomes. 15. Collect a number of testing fundus images. $SI_1, SI_2, SI_3, \ldots SI_n$ taken at the input layer 16. For each testing image SI 17. Formulate the neuron activation probability using (2) 18. Preprocessing the input image using (3) (4) –[hidden layer 1] 19. Segment the ROI using (5)(6) 20. Extracts the clinical features using (7)(8)(9)(10) 21. End for 22. Measure the congruence correlation coefficient using (14) 23. Obtain the classification results 24. Visualize the infected region by applying gradient class activation using (19) 25. For each classification outcome 26. Compute the error rate 'ε' using (20) 27. Update the weight using (21) 28. End for 29. Repeat the process until you find the minimum error 30. Obtain the final disease prediction results at the output layer End

Algorithm 1 illustrates GWCAMDTL with high accuracy and minimal time consumption.

4. Experimental Scenario

The proposed GWCAMDTL method and [1, 2] are implemented using the Python high-level programming language in the Glaucoma Fundus Imaging Dataset. For experimental consideration, 2000 images are considered.

5. Performance Comparison

Performance comparison of the GWCAMDTL method and [1, 2] is discussed with various parameters.

5.1 Performance Metrics

Accuracy'Acc': It is defined as the ratio of correct disease predictions made. It is measured in percentage (%).

$$\text{Acc} = \frac{\text{TP+TN}}{\text{TP+TN+FP+FN}} * 100 \quad (22)$$

Where, 'TP' is true positive, TN is true negative, 'FP' is false positive, FN is false negative.

Precision 'PC': it is measured as a ratio of true positives to the sum of true and false positives.

$$\text{PC} = \left(\frac{\text{TP}}{\text{TP+FP}}\right) \quad (23)$$

Sensitivity: it is also called recall, which is measured as the ratio of true positives to the sum of true positives and false positives results obtained in the disease prediction.

$$\text{Sensitivity} = \left(\frac{\text{TP}}{\text{TP+FN}}\right) \quad (24)$$

F1-score: This metric combines precision and recall into a single value.

$$\text{F1} - \text{score} = 2 * \left(\frac{\text{PC*Sensitivity}}{\text{PC+Sensitivity}}\right) \quad (25)$$

Specificity: It is the ratio of true negatives to the sum of true negatives and false positives.

$$\text{Specificity} = \left(\frac{\text{TN}}{\text{TN+FP}}\right) \quad (26)$$

Error rate: It is the percentage of all predictions that are incorrect, both FP and FN. It is measured in percentage (%).

$$\text{Error rate} = \left(\frac{\text{FN+FP}}{\text{TP+TN+FP+FN}}\right) \quad (27)$$

Prediction time'PT': It is defined as the time taken by the algorithm. It is measured in milliseconds (ms).

$$\text{PT} = \sum_{i=1}^{n} \text{SI}_i * \text{TM(PS)}] \quad (28)$$

Where n is the number of sample images 'SI', TM is the time for predicting one image sample (PS).

Table 2 and Figure 6 depict glaucoma disease prediction accuracy and precision. The accuracy of the GWCAMDTL method improved by 5% and 9% compared to [1, 2].

Table 2. Comparison of the accuracy

Number of Sample images	Accuracy (%)		
	GWCAMDTL	GDA	Glaucoma detection framework
200	98.5	93.5	92
400	97.56	93.05	91.75
600	96.78	92.41	90.03
800	95.52	91.02	88.44
1000	94.85	90.45	87.03
1200	93.89	89.45	85.45
1400	93.08	88.78	84.36
1600	94.56	89.45	85.43
1800	95.78	90.12	87.56
2000	97.12	92.02	89.05

Table 3. Comparison of the precision

Number of Sample images	Precision		
	GWCAMDTL	GDA	Glaucoma detection framework
200	0.983	0.942	0.925
400	0.974	0.93	0.915
600	0.966	0.925	0.907
800	0.952	0.918	0.902
1000	0.945	0.904	0.885
1200	0.938	0.897	0.872

1400	0.922	0.885	0.865
1600	0.935	0.905	0.884
1800	0.945	0.922	0.89
2000	0.964	0.934	0.9

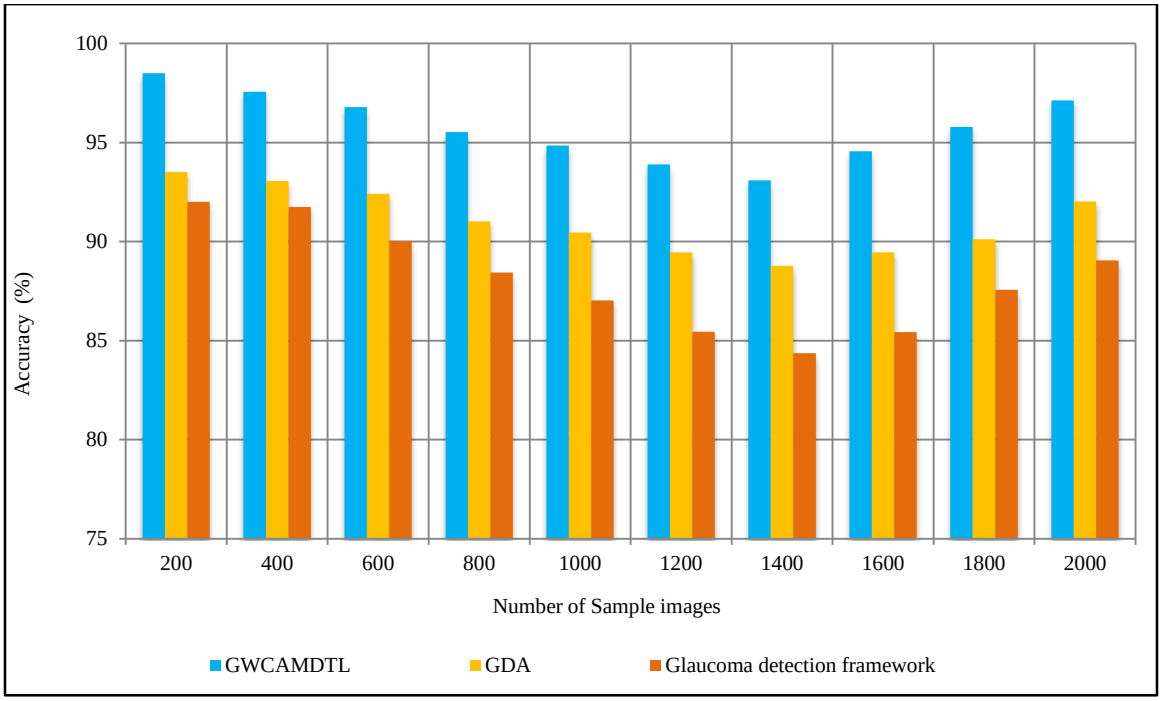

Fig. 6 Graphical Representations of accuracy

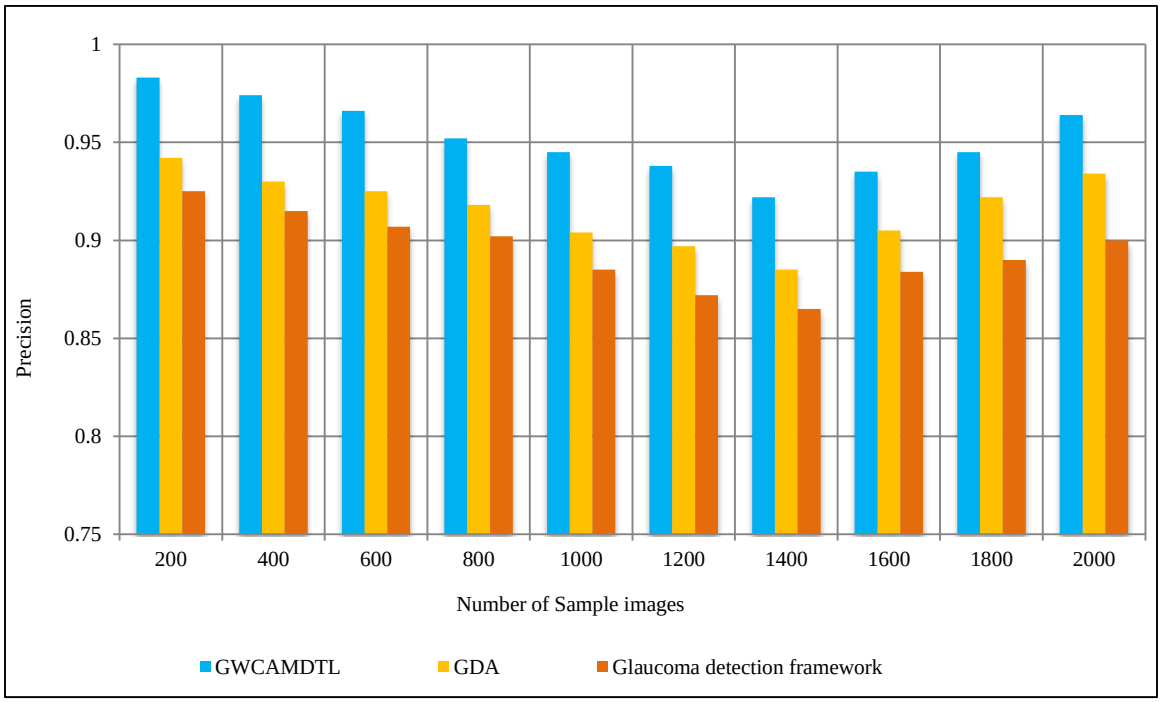

Fig. 7 Graphical representations of precision

Table 3 and Figure 7 demonstrate precision. Precision improved by 4% compared to [1] and 6% compared to [2] with GWCAMDTL. To achieve enhanced performance, GWCAMDTL employs a deep transfer learning model.

Table 4. Comparison of the sensitivity

Number of Sample images	Sensitivity		
	GWCAMDTL	GDA	Glaucoma detection framework
200	0.991	0.95	0.941
400	0.985	0.942	0.922
600	0.972	0.933	0.91
800	0.963	0.925	0.9
1000	0.955	0.915	0.88
1200	0.945	0.902	0.87
1400	0.933	0.897	0.86
1600	0.952	0.918	0.875
1800	0.965	0.928	0.889
2000	0.984	0.939	0.905

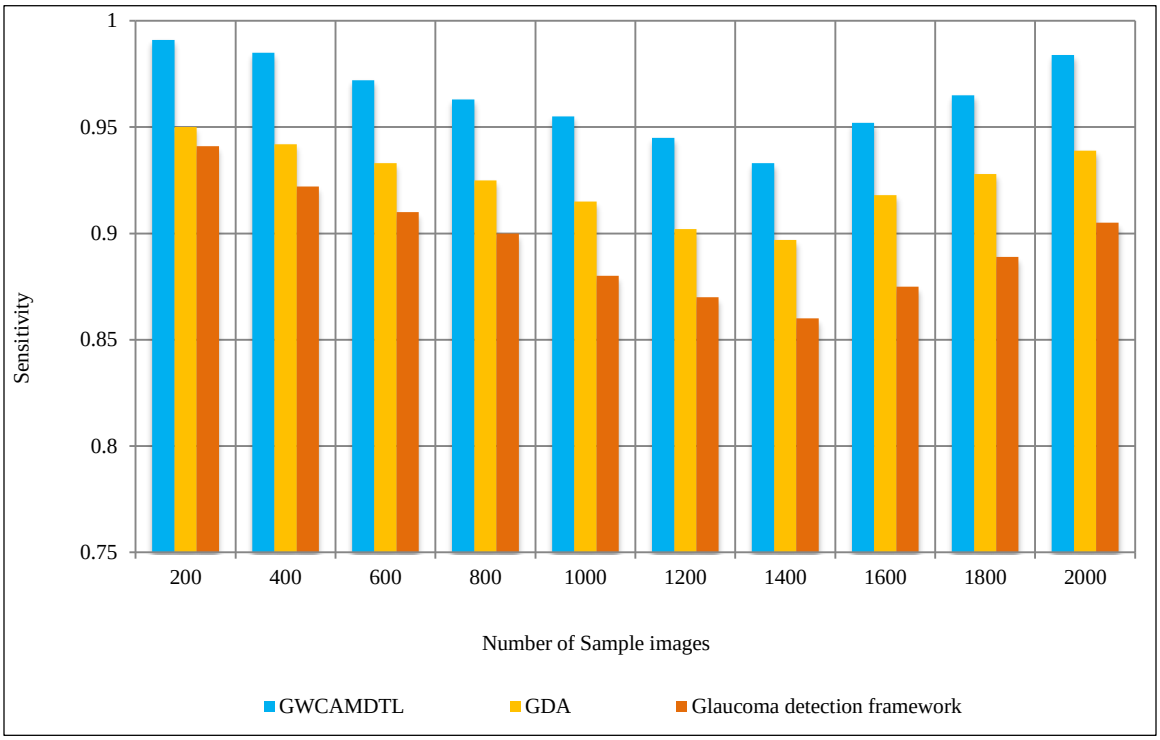

Fig. 8 Graphical Representations of Sensitivity

Table 4 and Figure 8 illustrate sensitivity. Sensitivity improved by 4% and 8% than [1, 2].

Table 5. Comparison of the F1 score

Number of Sample images	F1 score		
	GWCAMDTL	GDA	Glaucoma detection framework
200	0.986	0.945	0.932
400	0.979	0.935	0.918
600	0.968	0.928	0.908
800	0.957	0.921	0.900
1000	0.949	0.909	0.882
1200	0.941	0.899	0.870
1400	0.927	0.890	0.862
1600	0.943	0.911	0.879
1800	0.954	0.924	0.889
2000	0.973	0.936	0.902

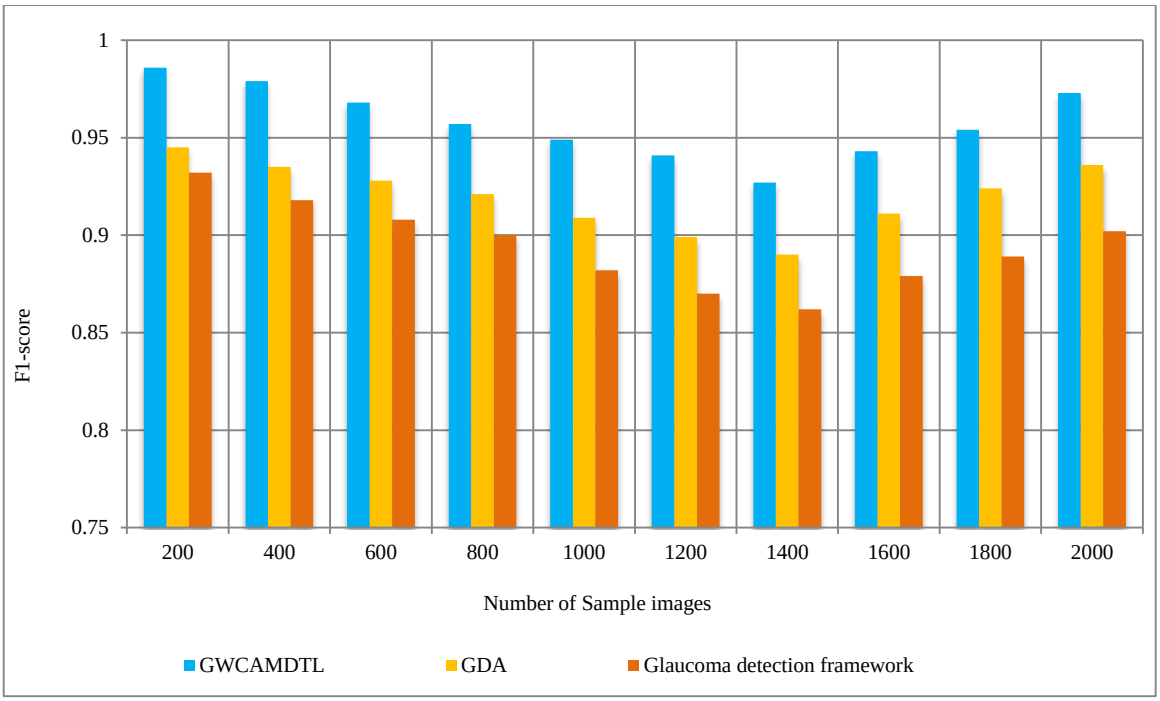

Fig. 9 Graphical representations of F1-score

Table 5 and Figure 9 demonstrate sensitivity and F1-score. F1-score of GWCAMDTL is improved by 4% and 7% than [1, 2].

Table 6 and Figure 10 illustrate specificity. The GWCAMDTL method increases specificity by 5% over [1] and 8% over [2].

Table 6. Comparison of the specificity

Number of Sample images	Specificity		
	GWCAMDTL	GDA	Glaucoma detection framework
200	0.974	0.912	0.888
400	0.965	0.905	0.872
600	0.947	0.9	0.865
800	0.938	0.895	0.874
1000	0.928	0.888	0.862
1200	0.917	0.875	0.854
1400	0.906	0.863	0.846
1600	0.928	0.895	0.874
1800	0.935	0.902	0.89
2000	0.947	0.918	0.9

Table 7. Comparison of the error rate

Number of Sample images	Error rate		
	GWCAMDTL	GDA	Glaucoma detection framework
200	0.015	0.065	0.08
400	0.024	0.069	0.082
600	0.032	0.075	0.099
800	0.044	0.089	0.115
1000	0.051	0.095	0.129
1200	0.061	0.105	0.145
1400	0.069	0.112	0.156
1600	0.054	0.105	0.145
1800	0.042	0.098	0.124
2000	0.028	0.079	0.109

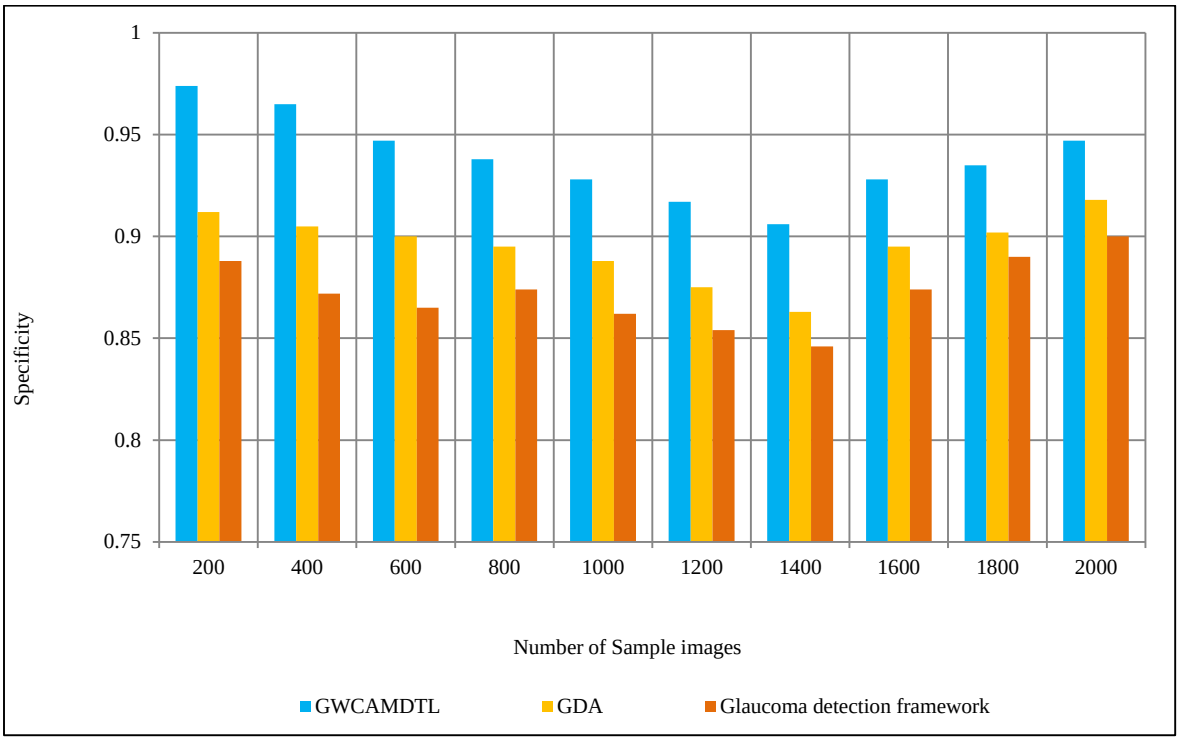

Fig. 10 Graphical Representations of Specificity

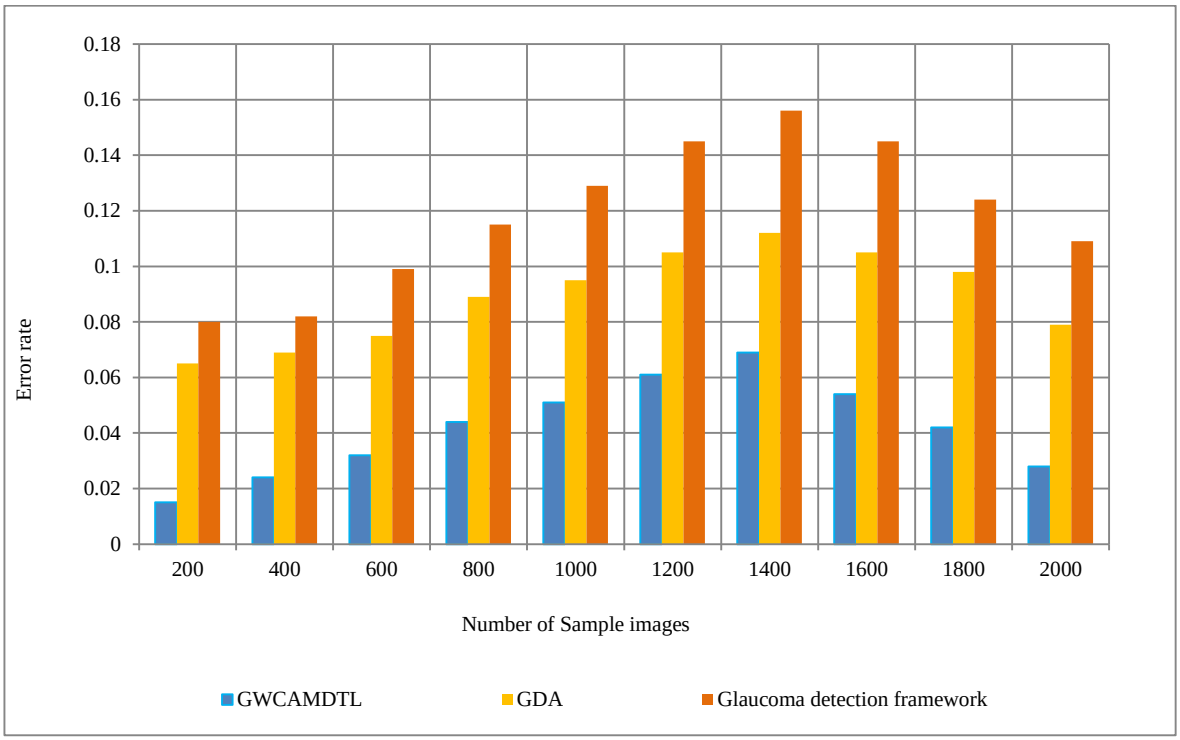

Fig. 11 Graphical representations of error rate

Table 7 and Figure 11 illustrate the error rate. GWCAMDTL reduces the error rate by 55% and 66% than [1, 2].

Table 8 and Figure 12 illustrate prediction time. GWCAMDTL of prediction time reduced by 12% and 16% than [1, 2].

Table 8. Comparison of the prediction time

Number of Sample images	Prediction time(ms)		
	GWCAMDTL	GDA	Glaucoma detection framework
200	16	19	20
400	18	22	23
600	20	24	25
800	23	26	28
1000	25	29	30
1200	28	31	33
1400	30	33	35
1600	33	36	37
1800	35	38	40
2000	39	41	42

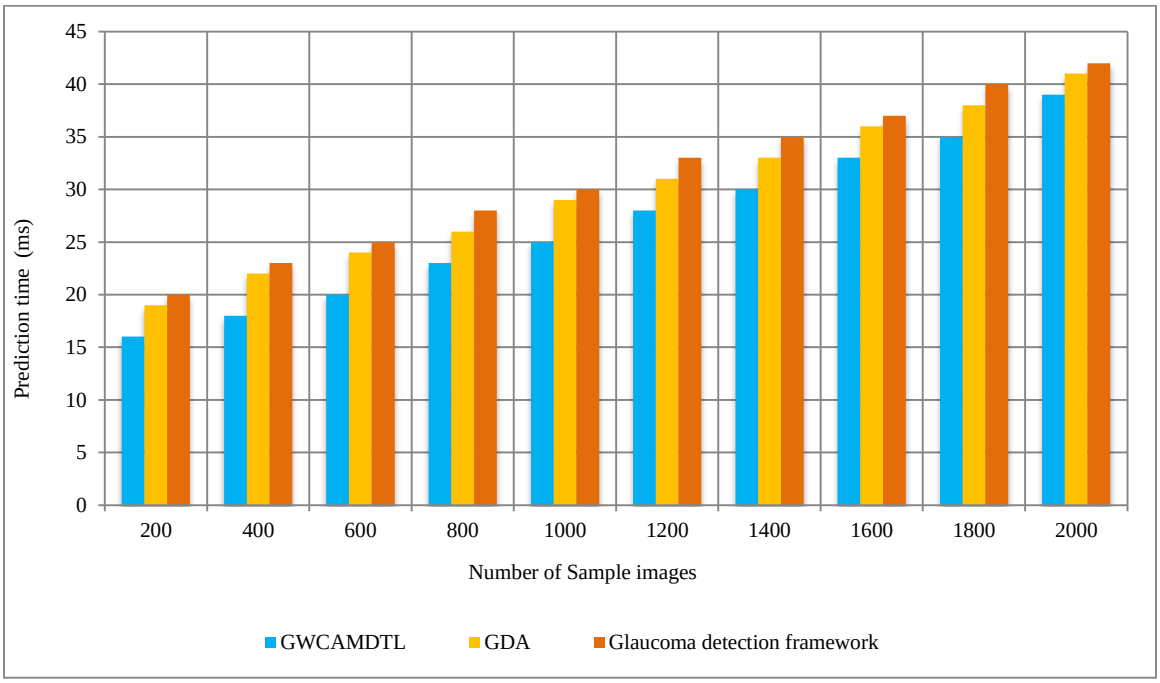

Fig. 12 Graphical representations of prediction time

5.2. Confusion matrix

A confusion matrix is a valuable tool in classification for evaluating the performance of GWCAMDTL. It summarizes prediction results by comparing actual (true) labels with predicted labels generated by the model.

Table 9. Confusion metrics using the GWCAMDTL method

	Total images 2000	Actual value		
		Positive	Negative	
Predicted value	Positive	TP=1650	FP=40	1690
	Negative	FN=20	TN=290	310
		1670	330	

Table 9 shows the confusion matrix of the proposed GWCAMDTL method using 2000 images.

5.3. Performance of the ROC curve

ROC (Receiver Operating Characteristic) curve evaluates the performance of the GWCAMDTL method, [1, 2] for predicting the positive class. It plots the True Positive Rate (TPR) against the False Positive Rate (FPR). Table 10 and Figure 13 present the ROC curve analysis of the proposed GWCAMDTL with [1, 2].

Table 10. Tabulation for ROC curve

FPR	TPR		
	GWCAMDTL	GDA	Glaucoma detection framework
0.1	0.12	0.08	0.065
0.2	0.35	0.25	0.18
0.3	0.46	0.37	0.32
0.4	0.62	0.52	0.46
0.5	0.75	0.63	0.57
0.6	0.82	0.7	0.65
0.7	0.89	0.8	0.76
0.8	0.96	0.88	0.82
0.9	0.98	0.92	0.86
1	0.99	0.95	0.89

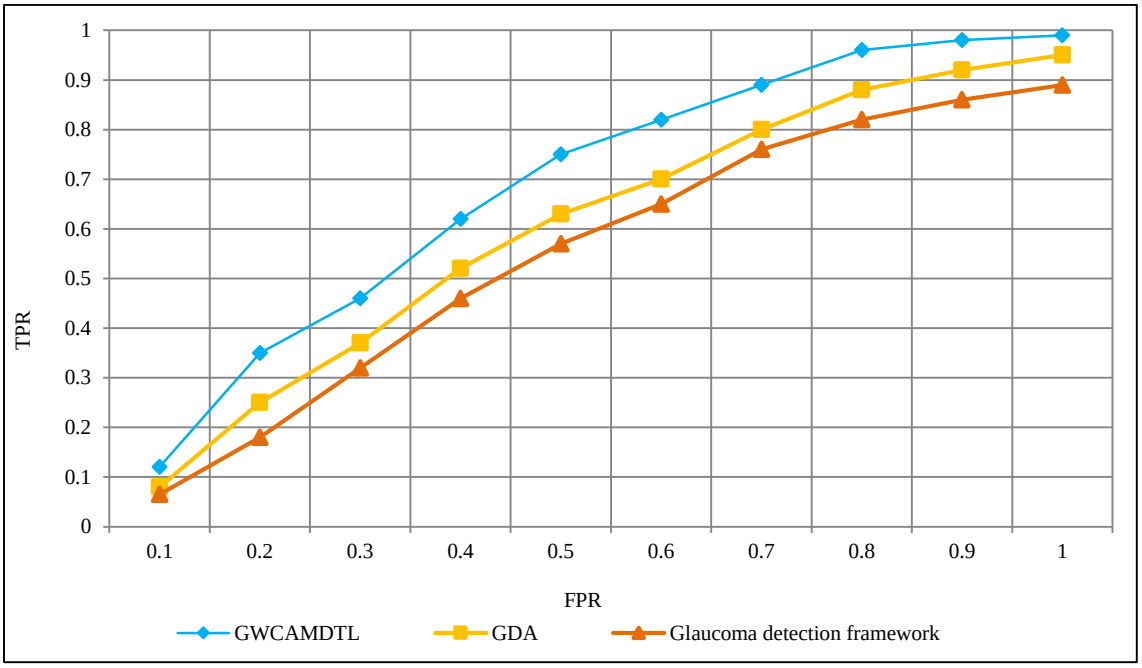

Fig. 13 Graphical representations of the ROC curve

6. Discussion

This study compares the proposed GWCAMDTL method and GDA [1], a Hybrid Glaucoma Detection Framework [2], using the Glaucoma Fundus Imaging Dataset based on different parameters, namely, accuracy, precision, recall, F1 -score, specificity, error rate, and prediction time with respect to sample images. Contrary to existing methods, the proposed GWCAMDTL provides finer results with maximum precision, recall, F1 -score, specificity, and lesser error and time. To achieve enhanced performance, the GWCAMDTL method employs a deep transfer learning model for performing image preprocessing, ROI segmentation, and feature extraction. Features are analyzed using the congruence correlation coefficient with the knowledge obtained from the pre-trained model to reduce time. This approach improves prediction accuracy by increasing the true positive rate and reducing false positives in glaucoma disease prediction. Fine-tunes weights between newly added layers used in transfer learning to minimize errors. Outcome of GWCAMDTL attains maximum accuracy by 96%, precision by 0.95, sensitivity by 0.96, F1 score by 0.95, and specificity by 0.93 with minimum time by 27% as well as error by 0.042 than state-of-the-art techniques.

7. Conclusion

In this paper, a novel prediction model called GWCAMDTL has been developed for early-stage glaucoma

detection using fundus images. The proposed GWCAMDTL method employs a transfer learning model to analyze input fundus images utilizing results from a pre-trained classification model. The GWCAMDTL method provides visual illustrations of the affected images following classification. The fine-tuning process of the transfer learning model further minimizes errors in disease prediction and enhances overall prediction accuracy. Experimental evaluation was conducted using various performance metrics. Results of proposed GWCAMDTL improve the accuracy of glaucoma disease prediction while reducing time and error rates compared to conventional methods.

Declarations

Funding

The authors declare that no funding was received for the research, authorship, and/or publication of this article.

Acknowledgment

None

Conflict of Interest

The authors declared that they have no conflicts of interest in this work.

Availability of data and material

The Glaucoma Fundus Imaging Dataset is used and publicly available within the article. It is taken from https://www.kaggle.com/datasets/arnavjain1/glaucoma-datasets

Code availability

Not applicable

Author contributions

The corresponding author claims the significant contribution of the paper, including formulation, analysis, and editing. The co-author provides guidance to verify the analysis result and manuscript editing.

References

[1] Yeganeh Madadi, Hashem Abu-Serhan, and Siamak Yousefi, "Domain Adaptation-based Deep Learning Models for Forecasting and Diagnosis of Glaucoma Disease," *Biomedical Signal Processing and Control*, vol. 92, pp. 1-14, 2024. [CrossRef] [Google Scholar] [Publisher Link]

[2] Abeer Aljohani, and Rua Y. Aburasain, "A Hybrid Framework for Glaucoma Detection Through Federated Machine Learning and Deep Learning Models," *BMC Medical Informatics and Decision Making*, vol. 24, no. 1, pp. 1-16, 2024. [CrossRef] [Google Scholar] [Publisher Link]

[3] Sumaiya Pathan et al., "An Automated Classification Framework for Glaucoma Detection in Fundus Images using Ensemble of Dynamic Selection Methods," *Progress in Artificial Intelligence*, vol. 12, no. 3, pp. 287-301, 2023. [CrossRef] [Google Scholar] [Publisher Link]

[4] Jahanzaib Latif et al., "ODGNet: A Deep Learning Model for Automated Optic Disc Localization and Glaucoma Classification using Fundus Images," *SN Applied Science*, vol. 4, no. 4, pp. 1-11, 2022. [CrossRef] [Google Scholar] [Publisher Link]

[5] Lucas Pascal et al., "Multi-Task Deep Learning for Glaucoma Detection from Color Fundus Images," *Scientific Reports*, vol. 12, no. 1, pp. 1-10, 2022. [CrossRef] [Google Scholar] [Publisher Link]

[6] Sajib Saha, Janardhan Vignarajan, and Shaun Frost, "A Fast and Fully Automated System for Glaucoma Detection using Color Fundus Photographs," *Scientific Reports*, vol. 13, no. 1, pp. 1-11, 2023. [CrossRef] [Google Scholar] [Publisher Link]

[7] N.K. Jisy et al., "Early Detection of Glaucoma: Feature Visualization with a Deep Convolutional Network," *Computer Methods in Biomechanics and Biomedical Engineering: Imaging and Visualization*, vol. 12, no.1, pp. 1-13, 2024. [CrossRef] [Google Scholar] [Publisher Link]

[8] Adnan Haider et al., "Artificial Intelligence-based Computer-Aided Diagnosis of Glaucoma using Retinal Fundus Images," *Expert Systems with Applications*, vol. 207, pp. 1-25, 2022. [CrossRef] [Google Scholar] [Publisher Link]

[9] Ali Raza et al., "Assisting Glaucoma Screening Process using Feature Excitationand Information Aggregation Techniques in Retinal Fundus Images," *Mathematics*, vol. 11, no. 2, pp. 1-20, 2023. [CrossRef] [Google Scholar] [Publisher Link]

[10] Mingquan Lin et al., "Automated Diagnosing Primary Open-Angle Glaucoma from Fundus Image by Simulating Human's Grading with Deep Learning," *Scientific Reports*, vol. 12, no. 1, pp. 1-10, 2022. [CrossRef] [Google Scholar] [Publisher Link]

[11] Rohit Thanki, "A Deep Neural Network and Machine Learning Approach for Retinal Fundus image Classification," *Healthcare Analytics*, vol. 3, pp. 1-9, 2023. [CrossRef] [Google Scholar] [Publisher Link]

[12] Thisara Shyamalee et al., "Automated Tool Support for Glaucoma Identification with Explainability using Fundus Images," *IEEE Access*, vol. 12, pp. 17290-17307, 2024. [CrossRef] [Google Scholar] [Publisher Link]

[13] Ahlam Shamsan, Ebrahim Mohammed Senan, and Hamzeh Salameh Ahmad Shatnawi, "Automatic Classification of Colour Fundus Images for Prediction Eye Disease Types based on Hybrid Features," *Diagnostics*, vol. 13, no. 10, pp. 1-23, 2023. [CrossRef] [Google Scholar] [Publisher Link]

[14] Xiaoling Huang et al., "GRAPE: A Multi-Modal Dataset of Longitudinal Follow-Up Visual Field and Fundus Images for Glaucoma Management," *Scientific Data*, vol. 10, no. 1, pp. 1-10, 2023. [CrossRef] [Google Scholar] [Publisher Link]

[15] Thisara Shyamalee, and Dulani Meedeniya, "Glaucoma Detection with Retinal Fundus Images using Segmentation and Classification," *Machine Intelligence Research*, vol. 19, no. 6, pp. 563-580, 2022. [CrossRef] [Google Scholar] [Publisher Link]

[16] You-Sang Cho et al., "Attention Mechanism-based Glaucoma Classification Model using Retinal Fundus Images," *Sensors*, vol. 24, no. 14, pp. 1-9, 2024. [CrossRef] [Google Scholar] [Publisher Link]

[17] Xiaoyan Hu et al., "GLIM-Net: Chronic Glaucoma ForecastTransformer for Irregularly Sampled Sequential Fundus Images," *IEEE Transactions on Medical Imaging*, vol. 42, no. 6, pp. 1875-1884, 2023. [CrossRef] [Google Scholar] [Publisher Link]

[18] Sanli Yi et al., "MTRA-CNN: A Multi-Scale Transfer Learning Framework for Glaucoma Classification in Retinal Fundus Images," *IEEE Access*, vol. 11, pp. 142689-142701, 2023. [CrossRef] [Google Scholar] [Publisher Link]

[19] Carlos A. Vásquez-Rochín et al., "Multi-Stage Ensemble-based System for Glaucomatous Optic Neuropathy Diagnosis in Fundus Images," *Electronics*, vol. 12, no. 4, pp. 1-15, 2023. [CrossRef] [Google Scholar] [Publisher Link]

[20] Xiaoyi Raymond Gao et al., "Automated Vertical Cup-to-Disc Ratio Determination from Fundus Images for Glaucoma Detection," *Scientific Reports*, vol. 14, no. 1, pp. 1-10, 2024. [CrossRef] [Google Scholar] [Publisher Link]

[21] Thangam Palaniswamy, and Mahendiran Vellingiri, "Internet of Things and Deep Learning Enabled Diabetic Retinopathy Diagnosis using Retinal Fundus Images," *IEEE Access*, vol. 11, pp. 27590-27601, 2023. [CrossRef] [Google Scholar] [Publisher Link]

[22] Shumoos Al-Fahdawi et al., "Fundus-Deep Net: Multi-Label Deep Learning Classification System for Enhanced Detection of Multiple Ocular Diseases Through Data Fusion of Fundus Images," *Information Fusion*, vol. 102, pp. 1-11, 2024. [CrossRef] [Google Scholar] [Publisher Link]

[23] K. Alice et al., "Effect of Multi Filters in Glucoma Detection using Random Forest Classifier," *Measurement: Sensors*, vol. 25, pp. 1-7, 2023. [CrossRef] [Google Scholar] [Publisher Link]

[24] Shaista Hussai et al., "Predicting Glaucoma Progression using Deep Learning Framework Guided by Generative Algorithm," *Scientific Reports*, vol. 13, no. 1, pp. 1-14, 2023. [CrossRef] [Google Scholar] [Publisher Link]

[25] Ayesha Shoukat et al., "Automatic Diagnosis of Glaucoma from Retinal Images using Deep Learning Approach," *Diagnostics*, vol. 13, no. 10, pp. 1-17, 2023. [CrossRef] [Google Scholar] [Publisher Link]

[26] Yi Li et al., "A Transfer Learning-based Multimodal Neural Network Combining Metadata and Multiple Medical Images for Glaucoma Type Diagnosis," *Scientific Reports*, vol. 13, no. 1, pp. 1-13, 2023. [CrossRef] [Google Scholar] [Publisher Link]

[27] Vijaya Kumar Velpula et al., "Glaucoma Detection with Explainable AI using Convolutional Neural Networks based Feature Extraction and Machine Learning Classifiers," *IET Image Processing*, vol. 18, no. 13, pp. 3827-3853, 2024. [CrossRef] [Google Scholar] [Publisher Link]

[28] Anita Desiani et al., "Multi-Stage CNN: U-Net and Xcep-Dense of Glaucoma Detection in Retinal Images," *Journal of Electronics, Electromedical Engineering, and Medical Informatics*, vol. 5, no. 4, pp. 211-222, 2023. [CrossRef] [Google Scholar] [Publisher Link]

[29] Cemil Közkurt et al., "Trish: An Efcient Activation Function for CNN Models and Analysis of its Effectiveness with Optimizers in Diagnosing Glaucoma," *The Journal of Supercomputing*, vol. 80, no. 11, pp. 15485-15516, 2024. [CrossRef] [Google Scholar] [Publisher Link]

[30] B.P. Pradeep kumar, Pramod K.B. Rangaiah, and Robin Augustine, "Enhanced Glaucoma Detection using U-Net and U-Net+ Architectures using Deep Learning Techniques," *Photodiagnosis and Photodynamic Therapy*, vol. 54, pp. 1-19, 2025. [CrossRef] [Google Scholar] [Publisher Link]

[31] Maheen Anwar et al., "E-GlauNet: A CNN-based Ensemble Deep Learning Model for Glaucoma Detection and Staging using Retinal Fundus Images," *Computers, Materials and Continua*, vol. 84, no. 2, pp. 3477-3502, 2025. [CrossRef] [Google Scholar] [Publisher Link]

[32] Venkatesh Guntreddi, and V. Sivakumar, "Deep Learning based Glaucoma Detection using Majority Voting Ensemble of ResNet50, VGG16, and Swin Transformer," *Results in Engineering*, vol. 28, pp. 1-13, 2025. [CrossRef] [Google Scholar] [Publisher Link]